Asian Journal of Chemistry; Vol. 38, No. 9 (2026), 2455-2462
ASIAN JOURNAL OF CHEMISTRY
https://doi.org/10.14233/ajchem.2026.36379

Synthesis and Spectroscopic Characterization of DTPA-*Bis* Anhydride-Tyramine Derived Metal Complexes: UV-Visible, Photoluminescence Studies and Cytotoxic Evaluations

B. NANDINI and M. AMUTHA SELVI*,

Department of Chemistry, Avinashilingam Institute for Home Science and Higher Education for Women, Coimbatore-641043, India

*Corresponding author: E-mail: amuthaselvi_chem@avinuty.ac.in

Received: 9 May 2026 *Accepted*: 18 August 2026 *Published online*: 5 September 2026 AJC-22474

In this study, 6,9-*bis*(carboxymethyl)-3-(2-((4-hydroxyphenethyl)amino)-2-oxoethyl)-14-(4-hydroxyphenyl)-11-oxo-3,6,9,12-tetraazatetradecanoic acid (DTPATY) was synthesized through the condensation of DTPA bisanhydride with tyramine in DMF under a nitrogen atmosphere. The corresponding metal complexes, [M(DTPATY)Cl_2] (M = Fe^{2+}, Cu^{2+}, Co^{2+}, Ni^{2+}, Mg^{2+} and Mn^{2+}), were prepared using $NaHCO_3$ under similar condensation conditions. The synthesized ligand and metal complexes were characterized by ESI-MS, elemental (CHN) analysis, FT-IR, UV-Vis and photoluminescence spectroscopy, while the ligand was further characterized by ^1H and ^{13}C NMR spectroscopy and the metal complexes by ESR spectroscopy. The spectroscopic and analytical data confirmed the formation of the DTPATY ligand and its coordination with the respective metal ions. Frontier molecular orbital (FMO) parameters were evaluated using density functional theory (DFT) at the B3LYP/6-31G′ level. The DTPATY ligand and its metal complexes exhibited favourable water solubility, distinct optical properties and low cytotoxicity, with the PL studies providing evidence of their fluorescence characteristics.

Keywords: DTPA derivative, Tyramine, Metal complexes, Spectroscopic techniques, MTT assay.

INTRODUCTION

Fluorescence-based techniques are widely used in the chemical and medicinal research owing to their high sensitivity, selectivity and suitability for real-time analysis. Among the molecular systems explored for fluorescence-related applications, diethylenetriaminepentaacetic acid (DTPA) has attracted considerable interest due to its strong and versatile coordination ability toward a range of metal ions [1-5]. DTPA contains multiple nitrogen and oxygen donor atoms that facilitate the formation of stable metal complexes with diverse coordination environments. DTPA incorporation into fluorescent systems can modulate their optical and physico-chemical properties, enabling the conjugation of fluorescent labels to biomolecules for targeted imaging and detection of organs, tissues and cells. DTPA-metal complexes have likewise been explored as contrast-enhancing agents for medical imaging by altering the properties of surrounding water protons and consequently, imaging signals [6-11].

The biological and physico-chemical properties of metal complexes are governed by the ligand framework, donor atoms and metal-ion characteristics. Transition-metal complexes are particularly relevant to sensing, analytical and optical applications owing to their diverse coordination geometries, accessible oxidation states and distinctive electronic structures [12,13]. DTPA is a multidentate aminopolycarboxylate ligand containing nitrogen and oxygen donor atoms that can form stable metal chelates, with the coordination environment and ligand architecture influencing the thermodynamic and kinetic properties of the resulting complexes [14,15].

Tyramine is a biologically relevant monoamine containing a phenolic hydroxyl group and an ethylamine side chain. It is structurally related to dopamine and noradrenaline and has been investigated in relation to a possible independent neurotransmitter system [16,17]. Tyramine is a trace biogenic amine found in peripheral tissues and the human brain and is also present in a range of raw and fermented foods, such as fish, meat, fruits, cheese, soybean-derived products and wine [18-20]. Its phenolic and amine functionalities provide suitable coordination and functionalization sites for the development of biologically relevant molecular systems.

In the present study, tyramine was conjugated with DTPA bisanhydride to obtain the ligand DTPATY, which was subsequently coordinated with the selected biologically relevant metal ions Fe^{2+}, Mg^{2+}, Co^{2+}, Mn^{2+}, Ni^{2+} and Cu^{2+} to obtain six new DTPATY-derived metal complexes. Although DTPA based metal complexes have been extensively investigated, systematic studies of DTPATY and its corresponding metal complexes remain limited. The ligand and metal complexes were characterized using FT-IR, ^{1}H NMR, ^{13}C NMR, ESR, UV-Vis and photoluminescence spectroscopy. Density functional theory (DFT) calculations were performed to examine their electronic structures and frontier molecular orbital characteristics, while *in vitro* cytotoxicity studies were conducted to assess their biological response. The combined experimental and computational approach established relationships among metal coordination, molecular structure, electronic properties, fluorescence behaviour and cytotoxicity. A tyramine-functionalized DTPA-bisanhydride ligand and six metal complexes were investigated to assess the influence of metal ions on their photophysical and biological properties, providing a basis for further fluorescence and bioanalytical studies.

EXPERIMENTAL

All chemicals were purchased from Sigma-Aldrich and TCI in analytical grade. The melting point of the ligand was determined by using melting point Apparatus (SAFIRE) using substance packed melting point tube with the heating rate of 10 ºC/min. the CHN elemental analysis was performed using CHN Elemental Analyzer-Perkin Elmer-2400. FTIR spectra were recorded in Shimadzu Prestige 20 IR spectrometer. ^{1}H (700 MHz) NMR spectra were recorded on Aligent DD2-700 MHz and ^{13}C NMR spectra were recorded on a Bruker Advance-III HD. ESR spectra of synthesized metal complexes were observed in JES-FA series spectrometer. Gaussian-16 and Gauss view software were used to calculate the molecular property of the ligand and B3LYP/6-31G' basic set was used. MTT assay for against cancer cells using colorectal cancer cell line and fibroblast mouse normal call line. Fluorescence and UV spectroscopy were analyzed on Perkin-Elmer Lambda-35for ligand and all corresponding complexes.

Synthesis of 6,9-*bis*(carboxymethyl)-3-(2-((4-hydroxyphenethyl)amino)-2-oxoethyl)-14-(4-hydroxyphenyl)-11-oxo-3,6,9,12-tetraazatetradecanoic acid: The DMF solution of DTPA-*bis* anhydride (2 mmol, 0.7147 g) was refluxed with tyramine (4 mmol, 0.5487 g) and a small amount of triethylamine (2 mL) was added in a mixture to maintain the pH (pH 8.2) of a solution. The mixture was refluxed for 8 h at 70 ºC under the nitrogen atmosphere to obtain honey brown colour solution (**Scheme-I**). The resulting ligand was separated and dried under vacuum. m.p.: 110 ºC, CHN analysis: calcd. (found) %: C, 57.04 (57.16); H, 6.54 (6.62); N, 11.09 (10.98); FTIR (KBr, ν_{max}, cm^{-1}): 3718.76 (OH), 3016.67 (arom.), 2314.58 (OH, acid), 1510.26 (C=O-NH), 1384.89 (C-N, amine), 1319.31 (C-O, acid), 1240.23 (C-N, DTPA); ^{1}H NMR (700 MHz, D_2O, δ ppm): 2.57 (d, 4H, N-CH_2-**CH_2**-N), 2.6 (d, 4H, N-**CH_2**-CH_2-N), 2.5 (S, 2H benzylic peak), 2.8 (d, 2H, NH-CH_2-**CH_2**-Ar), 2.9 (d, 2H, NH-**CH_2**-CH_2-Ar), 3.2 , 8H (t,

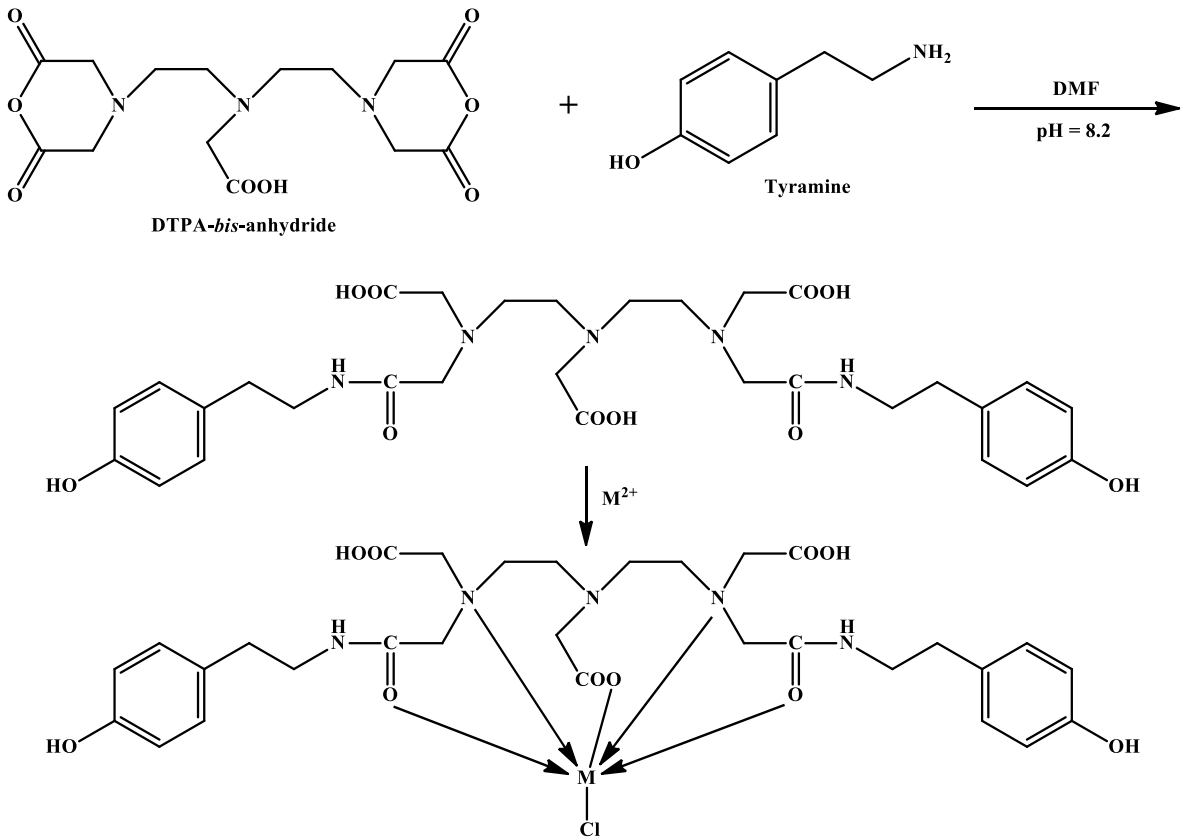

Scheme-I: Synthetic route of 6,9-*bis*(carboxymethyl)-3-(2-((4-hydroxyphenethyl)amino)-2-oxoethyl)-14-(4-hydroxyphenyl)-11-oxo-3,6,9,12-tetraazatetradecanoic acid (M = Cu, Fe, Mg, Ni, Mn and Co)

N-**CH₂**-COOH), 3.3 (S, 4H, N-**CH₂**-C=O-NH), 3.6 (S, 2H, N-**CH₂**-COOH), 6.6-6.7 (m, 8H, **Ar-H**), 7.02 (S, 2H, NH-C=O-**CH₂**), 7.03 (S, 2H, **NH-C=O**-CH_2); ^{13}C NMR (100 MHz, D_2O, δ ppm), 32.8-33.9 (C-N), 40.7, 58.1 (CH_2, C-H), 118.2-130.0 (Ar-C), 158, 163 (**C**=O acid), 174 (**C**=O amide); ESI-MS obtained (calcd.) = 630.7 + *m/z* ($[M+H]^+$), (631.6 *m/z*).

Synthesis of metal complexes: The 1:1 ratio of MCl_2 {where M = Cu(II), Fe(II), Co(II), Ni(II), Mg(II), Mn(II)} and DTPATY in $NaHCO_3$ and ligand mixture, refluxed over a water bath at 6 h. After completion of the reaction, the resulting solution was dried under vacuum (**Scheme-I**).

RESULTS AND DISCUSSION

The metal(II) complexes were obtained as coloured solids with varying yields and their physical characteristics are summarized in Table-1.

FT-IR studies: The FT-IR spectra of DTPATY and its metal(II) complexes were recorded to examine the functional groups and coordination behaviour of the synthesized complexes. The spectrum of DTPATY (Fig. 1a) exhibited strong bands at 1242 and 1388 cm^{-1}, attributed to C–N stretching vibrations associated with the DTPA bis-anhydride backbone [21-23]. A broad absorption band in the 3300-2500 cm^{-1} region arises from the overlapping O–H stretching vibrations of the phenolic and carboxylic acid groups [24,25]. The absorption at 1604 cm^{-1} is associated with the amide-I carbonyl (C=O) stretching vibration, while the band at 1510.26 cm^{-1} corresponds predominantly to the amide-II vibration arising from N–H bending coupled with C–N stretching. The presence of these bands supports the formation of amide linkages between DTPA bis-anhydride and tyramine [26]. The bands at 1442 and 1319 cm^{-1} are attributed to O–H bending and C–O stretching vibrations of the carboxylic acid groups, respectively [27].

The FT-IR spectra of the metal(II) complexes (Fig. 1b) exhibited distinct changes in the carboxylate and carbonyl regions rela-tive to the DTPATY ligand. A strong band in the 1620-1568 cm^{-1} region was assigned to the asymmetric stretching vibration of the carboxylate group, $\nu_{asym}(COO^-)$. This band overlaps with the amide-I carbonyl stretching vibration, preventing clear resolution of the two contributions. The symmetric carboxy-late stretching vibration, $\nu_{sym}(COO^-)$, appeared at 1402-1400 cm^{-1}. Owing to the overlap of ν_{asym} (COO^-) with the amide-I carbonyl band, a reliable Δν value [$\nu_{asym}(COO^-) - \nu_{sym}(COO^-)$] could not be determined [28]. The shifts observed in the carboxylate and carbonyl regions support the involvement of oxygen donor sites in metal coordination.

Weak absorptions in the 650-590, 416-349 and 402-389 cm^{-1} regions were observed for the metal(II) complexes and were assigned to M–O, M–N and M–Cl vibrations, respectively [29]. The spectral data are consistent with coordination of the metal centre through two nitrogen atoms of the DTPA backbone, two amide carbonyl oxygen atoms, one deprotonated carboxylate oxygen atom and one chloride ligand, giving a six-coordinate environment around the central metal ion [30].

^{1}H NMR studies: The structure of ligand DTPATY was examined by ^{1}H NMR spectroscopy in D_2O to confirm the

TABLE-1
PHYSICO-CHEMICAL DATA OF THE SYNTHESIZED METAL COMPLEXES

Complex	Colour of product	Yield (%)	CHN analysis	
			Calculated	Obtained
DTPATY-Cu	Ash green	40	C - 63.92%, H - 4.98%, N - 10.99%	C - 63.98%, H - 4.90%, N - 10.93%
DTPATY-Fe	Red brown	52	C - 64.90%, H - 5.18%, N - 10.96	C - 65.94%, H - 5.12%, N - 11.02%
DTPATY-Co	Russet brown	48	C - 49.68%, H - 5.57%, N - 9.68%	C - 49.70%, H - 5.56%, N - 9.66%
DTPATY-Ni	Chocolate brown	54	C - 49.73%, H - 5.53%, N - 9.68%	C - 49.71%, H - 5.56%, N - 9.66%
DTPATY-Mg	Wood brown	60	C - 65.95%, H - 5.19%, N - 11.01%	C - 65.94%, H - 5.11%, N - 10.95%
DTPATY-Mn	Honey brown	57	C - 65.99%, H - 5.13% N - 11.01%	C - 66.03%, H - 5.10%, N - 10.95%

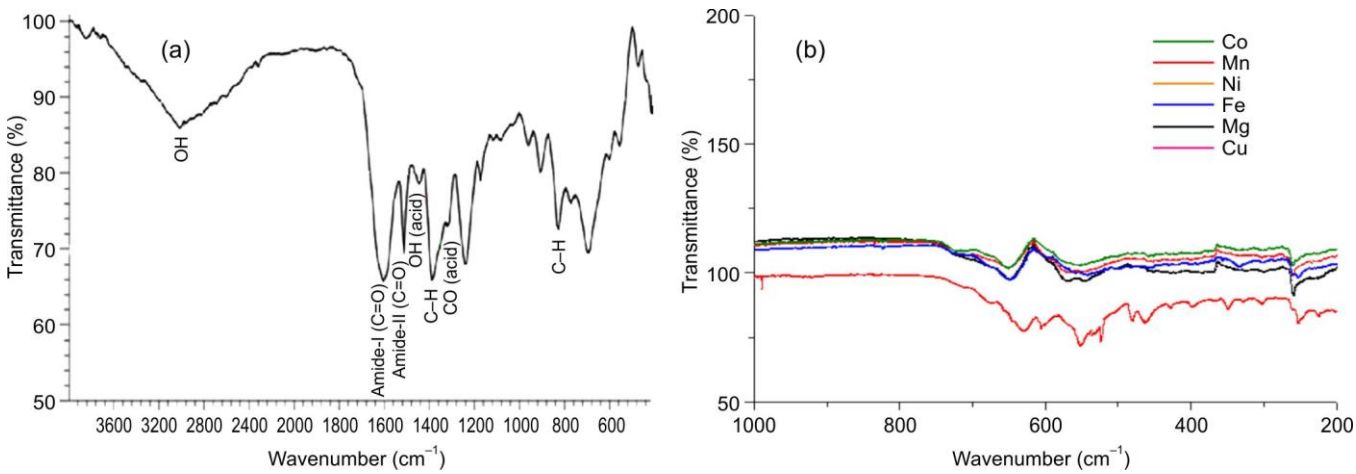

Fig. 1. (a) IR spectrum of 6,9-*bis*(carboxymethyl)-3-(2-((4-hydroxyphenethyl)amino)-2-oxoethyl)-14-(4-hydroxy phenyl)-11-oxo-3,6,9,12-tetraazatetradecanoic acid and (b) IR spectra of synthesized metal(II) complexes

formation of the synthesized ligand. The methylene protons adjacent to the nitrogen atoms of the DTPA backbone appeared as triplet signals at δ 2.5 and 2.7 ppm (t, 4H, N–CH_2). The CH_2 protons of the ethylene linker connecting the DTPA moiety to the tyramine unit resonated at δ 2.8 ppm (t, 4H, CH_2–CH_2–Ar). The methylene protons adjacent to the amide groups appeared as a singlet at δ 3.3 ppm (s, 4H, N–CH_2–C=O–NH), with the downfield position arising from the deshielding effect of the neighbouring carbonyl group (Fig. 2).

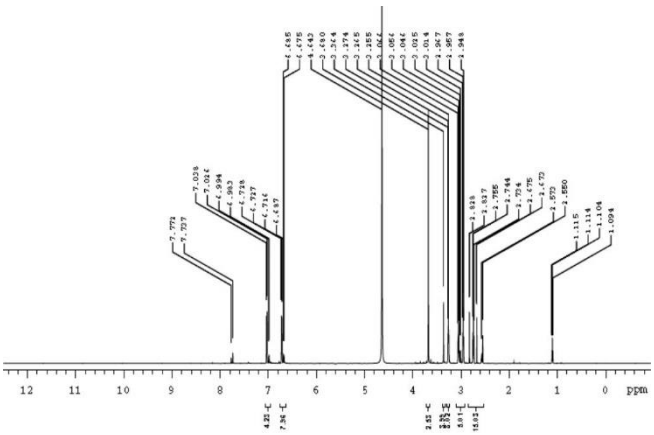

Fig. 2. ^{1}H NMR spectrum of 6,9-*bis*(carboxymethyl)-3-(2-((4-hydroxyphenethyl)amino)-2-oxoethyl)-14-(4-hydroxy phenyl)-11-oxo-3,6,9,12-tetraazatetradecanoic acid

A singlet at δ 3.6 ppm (s, 2H, N–CH_2–COOH) was assigned to the methylene protons adjacent to the carboxylic acid group. The electron-withdrawing nature of the –COOH group accounts for the relatively downfield position of this signal. Since the spectrum was recorded in D_2O, the exchangeable amide N–H proton was not observed owing to proton–deuterium exchange. The aromatic protons of the *para*-substituted tyramine ring appeared as overlapping signals in the δ 6.6-6.7 ppm region, assigned to the *ortho*- and *meta*-positioned aromatic protons (d, 4H and d, 4H, Ar–H). The observed splitting pattern is consistent with a *para*-substituted aromatic ring [31].

^{13}C NMR studies: The ^{13}C NMR spectrum of DTPATY (Fig. 3) exhibited multiple resonances in the δ 32.85-33.90 ppm, assigned to the methylene carbons of the DTPA bis-anhydride-derived framework (C–N). The relatively upfield chemical shifts are consistent with the shielding of these methylene carbons within the nitrogen-containing backbone. Signals at δ 158 and 163 ppm were assigned to the carboxylate/carboxylic acid carbon atoms. The amide carbonyl carbon (C=O) resonated at δ 174 ppm, supporting the formation of the amide linkage between the DTPA bis-anhydride moiety and tyramine. The methylene carbons of the tyramine linker, –CH_2–CH_2–Ar, appeared at δ 40.7 and 58.1 ppm. The aromatic carbon resonances occurred within the δ 118.2-130.2 ppm range, consistent with the *para*-substituted tyramine ring. The observed chemical-shift distribution arises from the different electronic environments of the aromatic carbons and the effects of the phenolic OH and ethylene substituents on the aromatic ring [27].

ESR spectral studies: The ESR spectra observed corresponding metal(II) complexes of [Cu(DTPATY)Cl_2] and

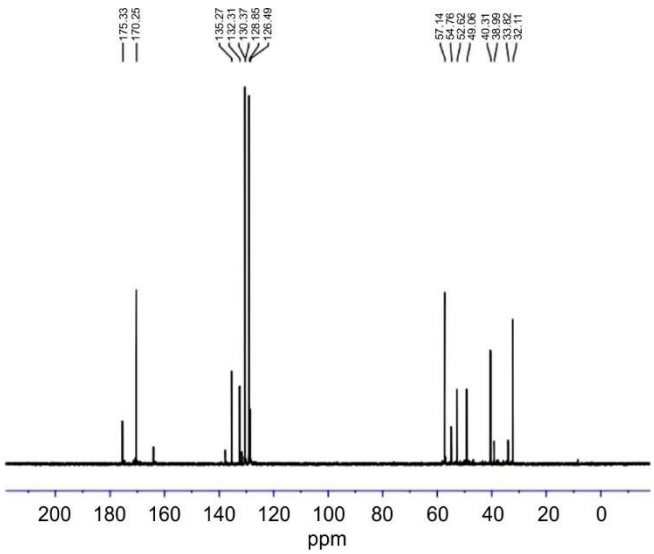

Fig. 3. ^{13}C NMR spectrum of 6,9-*bis*(carboxymethyl)-3-(2-((4-hydroxyphenethyl)amino)-2-oxoethyl)-14-(4-hydroxy phenyl)-11-oxo-3,6,9,12-tetraazatetradecanoic acid

[Mn(DTPATY)Cl_2] in X-band frequency (Fig. 4). In [Cu(DTPATY)Cl_2] complex shows, well resolved anisotropic signal and it (Cu^{2+} ion) have d^9 configuration. The g-value of this spectra, $g_{\|} \approx 2.23$ and $g_{\perp} \approx 2.08$, it indicates $g_{\|} > g_{\perp} > g_e$ (g_e – 2.0023 free electron value) in ground state of $d_{x\text{-}y}$ orbital with elongated octahedral geometry. The deviation of $g_{\|} \approx 2.23$ and constant free electron value g_e – 2.0023 indicates covalent character as the Cu complex's $g_{\|}$ value is good agreement with standard value of covalent bond $g_{\|} \approx 2.3$. So, [Cu(DTPATY)Cl_2] complex may have ligand-metal coordination through covalent bond to the oxygen and nitrogen atoms.

In contrast, [Mn(DTPATY)Cl_2] complex exhibits six-well resolved hyperfine lines from the interaction between the Mn nucleus and unpaired electrons. Using the hyperfine multiplicity rule 2I + 1 Mn-indicates (2I + 1 = 6) six-hyperfine lines, which is characteristic of the high spin $3d^5$-orbital in electronic configuration S = 5/2). The nearly isotropic g value and hyperfine splitting exhibits symmetrical ligand field around the Mn^{2+} ion environment. These characteristics are consistent with the octahedral coordination geometry. Therefore, observed ESR results proposed octahedral geometry of [Cu(DTPATY)Cl_2] and [Mn(DTPATY)Cl_2] complexes.

Frontier molecular orbital (FMO) analysis: The FMO energies provide insight into the electronic structure and reactivity of DTPATY (Fig. 5). The HOMO and LUMO energies were calculated as -0.19789 and -0.03068 a.u., respectively, giving an energy gap of 0.16721 a.u. The relatively small HOMO–LUMO gap is associated with lower kinetic stability and enhanced chemical reactivity. The comparatively high HOMO energy suggests favourable electron-donating ability, which may facilitate metal-ion coordination through the nitrogen and oxygen donor sites. The small energy gap may further favour intramolecular charge transfer and electronic excitation, contributing to the optical response of DTPATY and its metal complexes [32].

UV-Visible and photoluminescence studies: The optical properties of DTPATY and its metal(II) complexes were investigated by UV-Visible absorption and photoluminescence

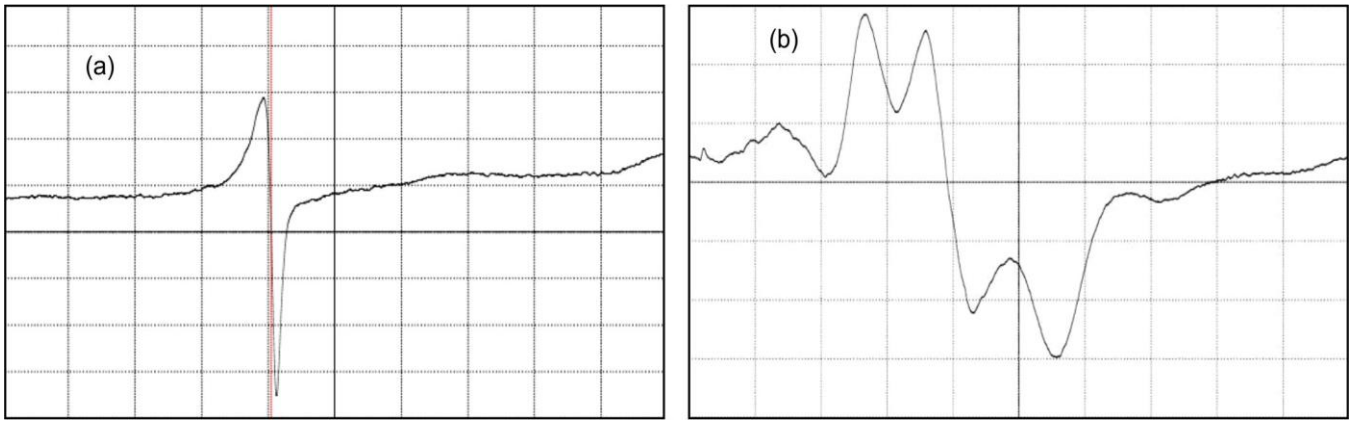

Fig. 4. ESR spectra of [Cu(DTPATY)Cl_2] and [Mn(DTPATY)Cl_2] complexes

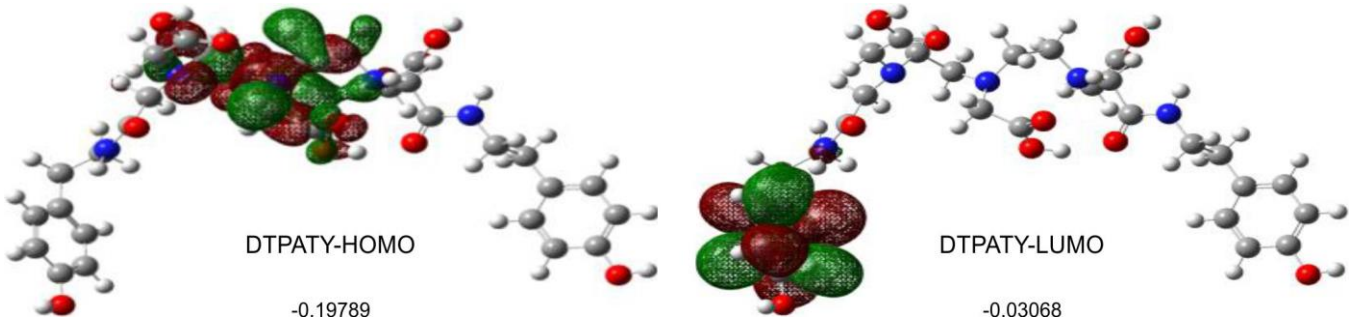

Fig. 5. HOMO-LUMO property of DTPATY

spectroscopy. Metal coordination can alter the electronic environment of the ligand and produce changes in absorption bands that provide information on the coordination process and electronic transitions [33]. DTPATY exhibited an absorption band at 270 nm, which can be associated with an (n→π*) transition involving the carbonyl-containing groups. The aromatic tyramine moiety gave a strong absorption in the 200-220 nm region, characteristic of a π→π transition. A weak feature near 260 nm was associated with the amide group, while a weak shoulder near 350 nm can be assigned to an (n→π*) transition involving the carboxylate/carbonyl groups of the DTPA-derived moiety. Following metal(II) coordination, no pronounced absorption bands were observed above approximately 350 nm. The changes in the absorption profile are consistent with modification of the ligand electronic environment upon complex formation.

The fluorescence behaviour of DTPATY and its metal(II) complexes was examined under UV irradiation at 365 nm (Fig. 6). DTPATY, Fe-DTPATY and Cu-DTPATY exhibited readily visible fluorescence, while Co-DTPATY and Mg-DTPATY showed moderate emission. Ni-DTPATY and Mn-DTPATY complexes displayed the strongest fluorescence responses among the investigated complexes. The emission spectra (Fig. 7b) further confirmed differences in fluorescence intensity and emission wavelength across the series. DTPATY exhibited an emission maximum near 300 nm with a fluorescence intensity of approximately 230 nm (Fig. 7a). Metal(II) coordination altered both the emission intensity and spectral profile, with Ni-DTPATY giving the highest emission intensity. The Ni(II) and Mn(II) complexes exhibited emission maxima near 295 and 300 nm, respectively. The position and intensity of these bands can be influenced by the aqueous polar environment in which the measurements were performed [34].

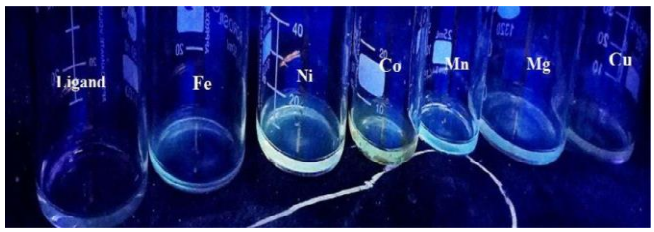

Fig. 6. DTPATY and its metal complexes were treated under UV light at 365 nm

The enhanced fluorescence observed for Ni-DTPATY may be associated with coordination-induced restriction of intramolecular rotation and vibration within the multidentate ligand framework. Such structural rigidification can reduce non-radiative relaxation and favour ligand-centred radiative decay, consistent with a chelation-enhanced fluorescence mechanism [35]. The observed emission is assigned predominantly to the DTPATY ligand rather than to a metal-centred excited state. Although Ni(II) complexes can undergo non-radiative processes associated with metal-centred states, the comparatively strong emission of Ni-DTPATY suggests that ligand-centred fluorescence remains significant in this system [35]. The differences in emission intensity among the complexes can be related to the influence of the coordinated metal ion on the excited-state dynamics of the DTPATY framework.

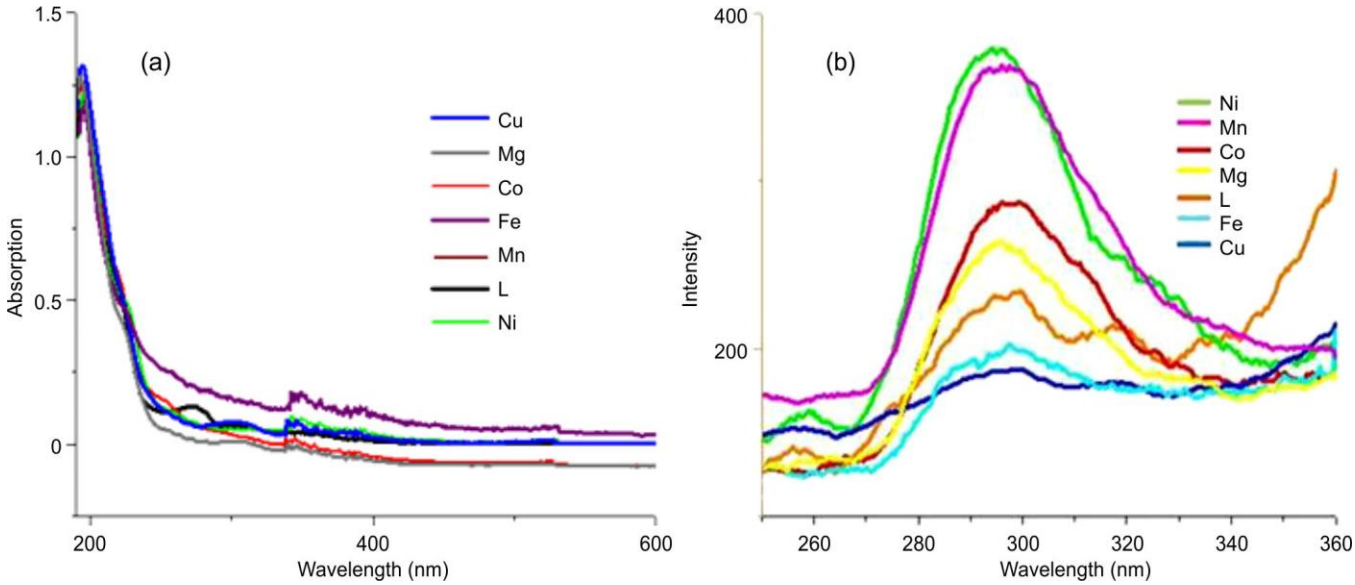

Fig. 7. UV spectra (a) and fluorescence spectra (b) of synthesized ligand and their metal(II) complexes

Cytotoxicity assay: The cytotoxicity of DTPATY and its metal(II) complexes was evaluated by the MTT assay using the human HT29 colorectal cancer cell line and the L-929 mouse fibroblast cell line as a normal-cell model. The cells were treated with each compound at concentrations of 50, 100 and 150 μg/mL. Among the tested compounds, Ni- DTPATY exhibited the highest reduction in HT29 cell viability, with viability decreasing to 58.87% at 150 μg/mL. The IC_{50} value of 195.38 μg/mL indicates a relatively weak cytotoxic response under the experimental conditions. The observed activity places the Ni(II) complex within the moderate-to-low cytotoxic range relative to the other synthesized complexes [36,37]. The cell-viability profiles of DTPATY and its metal(II) complexes are shown in Fig. 8.

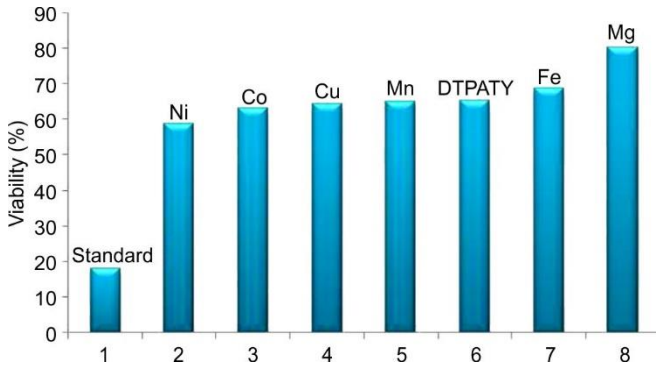

Fig. 8. Cell viability of DTPATY and its metal complexes

The cell viability was calculated using the following equation:

$$\text{Viability (\%)} = \frac{\text{Control OD} - \text{Sample OD}}{\text{Control OD}} \times 100$$

The cytotoxicity of DTPATY and its metal(II) complexes against the human HT29 colorectal cancer cell line and L-929 mouse fibroblast cell line, as evaluated by the MTT assay, is shown in Fig. 9.

Conclusion

DTPA-bis-anhydride was successfully conjugated with tyramine to obtain DTPATY, followed by the synthesis of its metal complexes. Spectroscopic characterization supported coordination of the metal ions through nitrogen and oxygen donor sites of the ligand, consistent with a six-coordinate environment around the metal centres. FMO analysis gave a HOMO-LUMO energy gap of 0.16721 a.u., placing DTPATY in a relatively reactive electronic regime with favourable electron-donating characteristics. Photoluminescence studies showed the highest emission intensity for the Ni-DTPATY complex among the investigated complexes, which may arise predominantly from ligand-centred emission influenced by metal coordination. In the MTT assay, Ni-DTPATY produced the highest reduction in HT29 cell viability, with 58.87% viability at 150 μg/mL and an IC_{50} value of 195.38 μg/mL. The fluorescence response and cytotoxic activity of Ni-DTPATY complex provide a basis for further investigation of its photophysical properties and biological behaviour.

CONFLICT OF INTEREST

The authors declare that there is no conflict of interests regarding the publication of this article.

DECLARATION OF AI-ASSISTED TECHNOLOGIES

During the preparation of this manuscript, the authors used an AI-assisted tool(s) to improve the language and no data, results or scientific conclusions were generated by AI. All analyses, interpretations and conclusions are the authors' own. The authors reviewed and edited the content and take full responsibility for the published work.

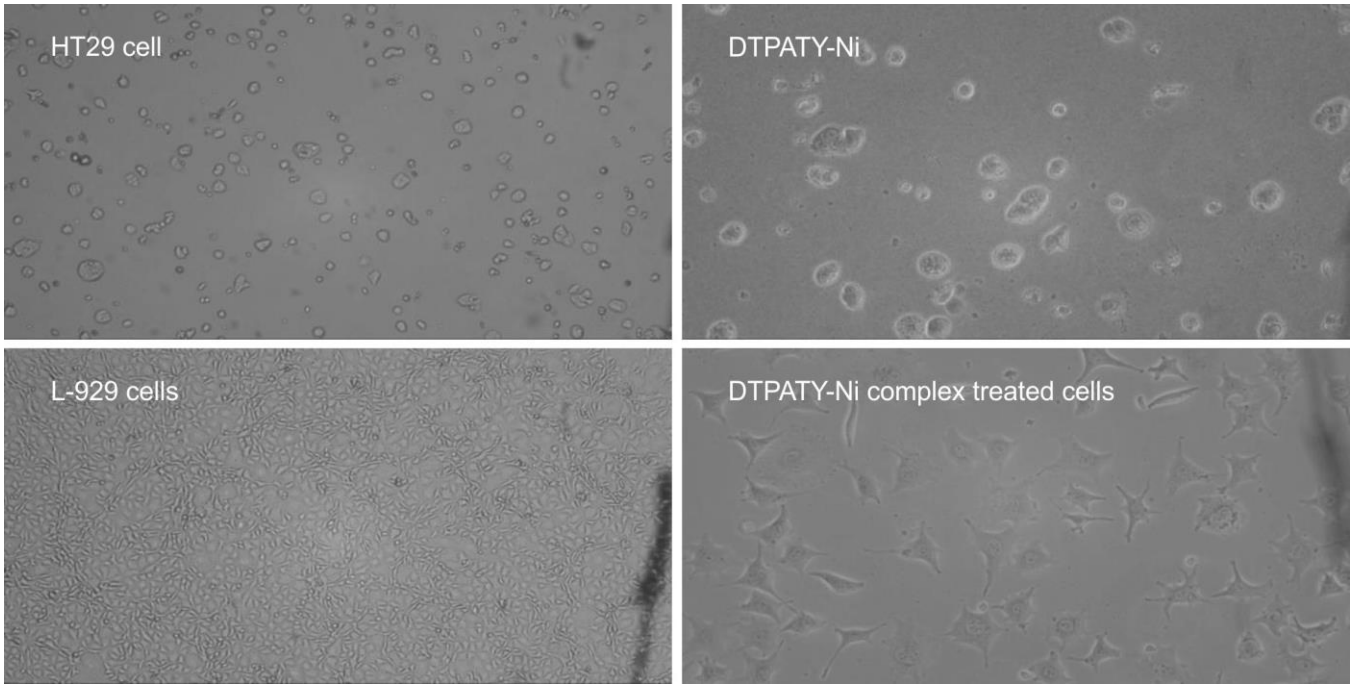

Fig. 9. The MTT assay resulted images of human HT29- colorectal cancer cell line and L-929 fibroblast mouse normal call line for DTPATY-Ni

REFERENCES

1. R. Sánchez-Fernández, I. Obregon-Gomez, A. Sarmiento, M.E. Vázquez and E. Pazos, *Chem. Commun.*, **60**, 12650 (2024); https://doi.org/10.1039/D4CC03205E
2. B.M. Rotermund, N.B. Beck, H.B. Wineinger, J.M. Sperling, G.P. Horne, J.P. Brannon, R. Greer and T. E. Albrecht, *Inorg. Chem.*, **64**, 5341 (2025); https://doi.org/10.1021/acs.inorgchem.4c05386
3. L.K. Chinen, K.P. Galen, K.T. Kuan, M.E. Dyszlewski, H. Ozaki, H. Sawai, R.S. Pandurangi, R.B. Dorshow R. Rajagopalan and F.G. Jacobs, *J. Med. Chem.*, **51**, 957 (2008); https://doi.org/10.1021/jm070842+
4. C.W. Sathiyajith, A.J. Hallett, A.J. Amoroso and P.G. Edwards, *RSC Adv.*, **7**, 38463 (2017); https://doi.org/10.1039/C7RA06946D
5. A.A. Vinogradov, P.D. Komarov, L.N. Puntus, I.V. Taydakov, K.A. Lyssenko, I.E. Nifant'ev, E.A. Varaksina and D.M. Roitershtein, *Inorg. Chim. Acta*, **533**, 120777 (2021); https://doi.org/10.1016/j.ica.2021.120777
6. E. Kanal, J.H. Maki, P. Schramm and L. Marti-Bonmati, *J. Magn. Reson. Imaging*, **61**, 52 (2025); https://doi.org/10.1002/jmri.29367
7. N.R. Zargari, F. Ebrahimi, M. Akhlaghi, D. Beiki, K. Abdi, M.A. Abbasi, S. Ramezanpour and S.M. Asghari, *Biomed. Pharmacother.*, **178**, 117189 (2024); https://doi.org/10.1016/j.biopha.2024.117189
8. M. Amutha Selvi, S.J. Sivasankari, E.M. Vinoliya and B. Nandini, *Indian J. Chem.*, **65**, 680 (2026); https://doi.org/10.56042/ijc.v65i7.14794
9. K. Dydak, T. Zalewski, M. Kempka, P. Florczak, G. Nowaczyk, Ł. Przysiecka, J. Jagielski, B. Loppinet, M. Banaszak and D. Flak, *J. Mater. Chem. B*, **12**, 12017 (2024); https://doi.org/10.1039/d4tb01684j
10. X. Ding, M. Qi, Y. Zhou, Y. Qi, D. Chen, X. Yang, C. Ji and Y. Yao, *Neurosci. Lett.*, **851**, 138170 (2025); https://doi.org/10.1016/j.neulet.2025.138170
11. L.L. Ruston, G.M. Robertson and Z. Pikramenou, *Chem. Asian J.*, **5**, 571 (2010); https://doi.org/10.1002/asia.200900367
12. Y. Nagaya, M. Kutsukake, S.I. Chigusa and A. Komatsu, *Neurosci. Lett.*, **329**, 324 (2002); https://doi.org/10.1016/S0304-3940(02)00596-7
13. V.W.-W. Yam, A.K.-W. Chan and E.Y.-H. Hong, *Nat. Rev. Chem.*, **4**, 528 (2020); https://doi.org/10.1038/s41570-020-0199-7
14. R.H. Elattar, S.F. El-Malla, A.H. Kamal and F.R. Mansour, *Coord. Chem. Rev.*, **501**, 215568 (2024); https://doi.org/10.1016/j.ccr.2023.215568
15. J. Oakes and C.G. van Kralingen, *J. Chem. Soc., Dalton Trans.*, 1133 (1984); https://doi.org/10.1039/DT9840001133
16. P. Caravan, J.J. Ellison, T.J. McMurry and R.B. Lauffer, *Chem. Rev.*, **99**, 2293 (1999); https://doi.org/10.1021/cr980440x
17. V. Glover, C.J. Pycock and M. Sandler, *Br. J. Pharmacol.*, **80**, 141 (1983); https://doi.org/10.1111/j.1476-5381.1983.tb11059.x
18. G. Andersen, P. Marcinek, N. Sulzinger, P. Schieberle and D. Krautwurst, *Nutr. Rev.*, **77**, 107 (2019); https://doi.org/10.1093/nutrit/nuy036
19. N. Saha Turna, R. Chung and L. McIntyre, *Heliyon*, **10**, e24501 (2024); https://doi.org/10.1016/j.heliyon.2024.e24501
20. P. Sadighara, S. Aghebat-Bekheir, H. Shafaroodi, B. Basaran, and M. Sadighara, *Food Prod. Process. Nutr.*, **6**, 30 (2024); https://doi.org/10.1186/s43014-024-00223-x
21. W. Liu, B. Wang, H. Jia, J. Wang and Y. Song, *New J. Chem.*, **43**, 16478 (2019); https://doi.org/10.1039/C9NJ03972D
22. Z. Yu, H. Jia, W. Liu, N. Li, J. Wang and Y. Song, *J. Photochem. Photobiol. A Chem.*, **383**, 111970 (2019); https://doi.org/10.1016/j.jphotochem.2019.111970
23. G. Arrachart, A. Kenaan, S. Gracia, R. Turgis, V. Dubois and S. Pellet-Rostaing, *Sep. Sci. Technol.*, **50**, 1882 (2015); https://doi.org/10.1080/01496395.2015.1012591
24. M. Silverstein, G.C. Bassler and T.C. Morrill, Spectrometric Identification of Organic Compounds, Wiley, edn. 5, p. 92 (1991); https://doi.org/10.1002/jps.2600800208
25. G. Ancora, S. Marchesi, M. Botta, L. Marchese, F. Carniato and C. Bisio, *Dalton Trans.*, **53**, 7801 (2024); https://doi.org/10.1039/D4DT00388H

26. K. Nakamoto, Infrared and Raman Spectra of Inorganic and Coordination Compounds, Wiley, edn 6, p. 248 (2009).
27. S. Laurent, T.N. Parac-Vogt, K. Kimpe, C. Thirifays, K. Binnemans, R.N. Muller and L. Vander Elst, *Eur. J. Inorg. Chem.*, **2007**, 2061 (2007); https://doi.org/10.1002/ejic.200601170
28. D. Lin-Vien, N.B. Colthup, W.G. Fateley and J.G. Grasselli, The Handbook of Infrared and Raman Characteristic Frequencies of Organic Molecules, Academic Press, Boston, MA, USA, pp. 277-306 (1991).
29. P.L. Pauson, Infrared Spectroscopy: Applications in Organic Chemistry, London, U.K.: Butterworths, p. 54 (1968).
30. R.M. Silverstein and F.X. Webster, Spectrometric Identification of Organic Compounds, Wiley, edn. 7, p. 89 (2005).
31. Z. Ma, N. Wang, K. Guo, X. Zheng and J. Lin, *Inorg. Chim. Acta*, **399**, 126 (2013); https://doi.org/10.1016/j.ica.2013.01.010
32. G.B. Deacon, *Coord. Chem. Rev.*, **33**, 227 (1980); https://doi.org/10.1016/S0010-8545(00)80455-5
33. D.L. Pavia, G.M. Lampman, G.S. Kriz and J.R. Vyvyan, Introduction to Spectroscopy, Cengage Learning, edn 5, p. 145 (2015).
34. A. Abragam and B. Bleaney, Electron Paramagnetic Resonance of Transition Ions, Clarendon Press, Oxford, pp. 338 (1970).
35. B. Saranya and M. Gowri, *J. Mol. Struct.*, **1250**, 131674 (2022); https://doi.org/10.1016/j.molstruc.2021.131674
36. F. Yang, P. Ren, G. Liu, Y. Song, N. Bu and J. Wang, *Spectrochim. Acta A Mol. Biomol. Spectrosc.*, **193**, 357 (2018); https://doi.org/10.1016/j.saa.2017.12.038
37. C. Diaferia, E. Gianolio, P. Palladino, F. Arena, C. Boffa, G. Morelli and A. Accardo, *Adv. Funct. Mater.*, **25**, 7003 (2015); https://doi.org/10.1002/adfm.201502458